PERGAMON

Applied Thermal Engineering 22 (2002) 873–883

APPLIED THERMAL ENGINEERING

www.elsevier.com/locate/apthermeng

A simulation of heat transfer during billet transport

Anton Jaklič [a,*], Branislav Glogovac [a], Tomaž Kolenko [b], Borut Zupančič [c], Bojan Težak [d]

[a] *Institute of Metals and Technology, Lepi pot 11, 1001 Ljubljana, Slovenia*
[b] *Faculty of Natural Science and Technology, University of Ljubljana, Aškrčeva 12, 1000 Ljubljana, Slovenia*
[c] *Faculty of Electrical Engineering, University of Ljubljana, Aškrčeva 12, 1000 Ljubljana, Slovenia*
[d] *Terming d.o.o., Ljubljana, Slovenia*

Received 1 October 2001; accepted 27 December 2001

Abstract

This paper presents a simulation model for billet cooling during the billet's transport from the reheating furnace to the rolling mill. During the transport, the billet is exposed to radiation, convection and conduction. Due to the rectangular shape of the billet, the three-dimensional finite-difference model could be applied to calculate the heat conduction inside the billet. The billets are reheated in a gas-fired walking-beam furnace and are exposed to scaling. The model takes into account the effect of the thin oxide scale. We proved that the scale significantly affects the temperature distribution in the billet and should not be neglected. The model was verified by using a thermal camera.

Keywords: Steel industry; Heat transfer; Billet cooling; Models

1. Introduction

Knowledge of the initial temperature field in a billet is very important for the quality of the hot-rolling process in the steel industry. The billet is reheated in a reheating furnace and then transported to the rolling mill. We have studied a new system for billet transportation from the reheating furnace to the rolling mill. It was built to allow one furnace to serve two rolling mills. The transport distance is about 70 m, and the time is about 54 s, depending on the system

* Corresponding author. Tel.: +386-1470-1999; fax: +386-1470-1939.
E-mail address: tone.jaklic@imt.si (A. Jaklič).

1359-4311/02/$ - see front matter
PII: S1359-4311(02)00022-4

Nomenclature

a temperature conduction $a = \lambda\rho^{-1}c^{-1}$ ($m^2 s^{-1}$)
A, B, C, D, E, F billet and scale surfaces
c specific heat capacity ($J kg^{-1} K^{-1}$)
d oxide-scale thickness (m)
∂ partial differential operator
L thickness in the void space in thermal contact (m)
MX, MY, MZ number of elements of the billet in corresponding x, y and z directions
$\dot{q}$ thermal flux ($W m^{-2}$)
Pr Prandtl number
Re Reynolds number
S area (m^2)
t time (s)
Δt calculation time interval (s)
T temperature (K)
u billet velocity ($m s^{-1}$)
v kinematic viscosity of fluid ($m^2 s^{-1}$)
x, y, z basic axis of 3D cartesian coordinate system
Δx, Δy, Δz billet element size in corresponding x, y and z directions (m)

Greeks
α heat transfer coefficient ($W m^{-2} K^{-1}$)
ε emissivity
λ thermal conductivity ($W m^{-1} K^{-1}$)
ρ density ($kg m^{-3}$)
σ Stefan–Boltzmann constant ($W m^{-2} K^{-4}$)

Subscripts
A, B, C, D, E, F billet and scale surfaces
AC, AF, CF scale edge
ACF scale corner
a surrounding air
b, billet billet
c contact
f fluid filling the void space
G air gap
i index in x direction
j index in y direction
k index in z direction
out to surrounding
r transport rolls

s	oxide scale
v	void space in thermal contact
w	water
Superscripts	
t	at time t
$t+\Delta t$	at time $t+\Delta t$

parameters. During this time, the billet temperature field is significantly changed; however, measuring methods do not give sufficient information on the billet temperature field. Optical pyrometers and thermal cameras only give data on the billet's surface temperature where the billet is visible, and trail thermocouples cannot be used because of the rapid movement of the billets. The most effective way of determining the whole billet temperature field is to use a simulation model. It allows us to experiment with easily changeable system parameters, i.e. different billet dimensions, different billet materials, different transport speeds, etc.

The three-dimensional finite-difference model was applied to calculate the heat conduction inside the billets. During the transport, billets are exposed to temperature-, time- and position-dependent boundary conditions.

The transport system consists of seven subsystems: the transport rolls from the furnace, the transport on the skids, the chain transport before descaling, the descaling, the billet rotation, the billet lift and the transport rolls to the rolling mill. Every subsystem has its own boundary conditions. The billet loses heat during the transport to the surroundings by radiation, by convection due to fast moving through the surrounding air, by thermal contact with the transport rolls and by water convection during the descaling process. The model includes all these different boundary conditions.

The billets are reheated in a gas-fired walking-beam furnace, where they are exposed to scale formation by oxidation. It is shown in [1] that the oxide scale significantly affects the temperature distribution in the billet. To include the effect of a thin oxide scale in the finite-difference model, the mesh had to be refined, which made the calculation time much longer. Therefore, three-dimensional finite-difference equations were derived for the thin oxide-scale elements around the billet. The developed equations for the scale allow the basic finite-difference model of the billet to remain unchanged and the calculation speed is only slightly decreased if the oxide scale is treated. When the billet is discharged from the furnace, the oxide scale starts cooling faster than the billet material. Therefore, it splits the billet and an air gap appears between the oxide scale and the billet. The model can also take into account calculations with an air gap between the oxide scale and the billet.

The purpose of the present work is to show the benefit of simulation techniques on high-temperature industrial processes, especially in cases where measuring techniques cannot be implemented. It is shown how the thin oxide scale can be treated with the three-dimensional finite-difference model. It is also shown that the oxide-scale treating should not be neglected in high-temperature heat-transfer simulations.

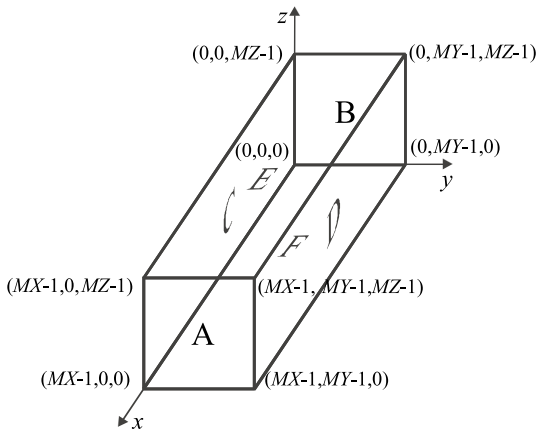

Fig. 1. Billet surfaces and corner elements.

2. Heat transfer in the billet

The main mechanism of heat transfer in the billet is thermal conduction. It is described by the heat-conduction partial differential equation:

$$\rho(T)c(T)\frac{\partial T}{\partial t} = \frac{\partial}{\partial x}\left[\lambda(T)\frac{\partial T}{\partial x}\right] + \frac{\partial}{\partial y}\left[\lambda(T)\frac{\partial T}{\partial y}\right] + \frac{\partial}{\partial z}\left[\lambda(T)\frac{\partial T}{\partial z}\right]$$

Due to rectangular shape of the billets, the three-dimensional finite-difference model has been employed to calculate the heat conduction inside the billets. The billet (length 3.50 m, width 0.14 m and height 0.14 m) is divided into a uniform rectangular mesh with MX (351) elements in the x direction, MY (15) elements in the y direction and MZ (15) elements in the z direction. The position of the billet in the coordinate system and the adequate corner elements of the billet are presented in Fig. 1.

The initial condition for the simulation is the temperature field in the billet at the time of discharge from the furnace. It is assumed in the model that the temperature field is uniform throughout the whole billet.

3. Boundary conditions

During transport, the billet is exposed to time- and position-dependent boundary conditions. In the model, the boundary conditions are presented as thermal fluxes $\dot{q}_{\text{out}}$. They can be different for each element of the billet or scale surface, depending on the temperature and the actual position of the element. At high temperatures, most of the heat is exchanged by radiation according to the Stefan–Boltzmann law [3]:

$$\dot{q}_{\text{out}} = \varepsilon_{\text{s}}\sigma(T_{\text{a}}^4 - T_{\text{s}}^4)$$

When the billet is moving, some of the heat is exchanged by convection, as suggested by [4]:

$$\dot{q}_{\text{out}} = \alpha_{\text{m}}(T_{\text{a}} - T_{\text{s}}), \quad \alpha_{\text{m}} = 0.332\frac{\lambda_{\text{a}}}{x}Pr^{1/3}Re_x^{1/2}, \quad Re_x = \frac{u_{\text{b}}x}{v_{\text{a}}}$$

During transport, there are some phases where the billet is stopped, i.e. prior to rotation or to change direction. In this case, free convection is present:

$$\dot{q}_{\text{out}} = \alpha_{\text{f}}(T_{\text{a}} - T_{\text{s}})$$

Besides these mechanisms of heat exchange, the billet exchanges heat with the transport rolls. The main mechanism in this situation is heat conduction. Because of the rapid movement, it is assumed that the exchanged heat is uniformly distributed on the billet or the oxide-scale contact surface (F), which is in thermal contact with the transport rolls. The thermal flux is calculated for the small area of the billet in direct thermal contact with the transport rolls as suggested by [2]:

$$\dot{q}_{\text{out}} = \frac{T_{\text{r}} - T_{\text{s}}}{1/\alpha_{\text{c}}}, \quad \alpha_{\text{c}} = \frac{1}{L_{\text{g}}}\left(\frac{S_{\text{c}}}{S}\frac{2\lambda_{\text{r}}\lambda_{\text{s}}}{\lambda_{\text{r}} + \lambda_{\text{s}}} + \frac{S_{\text{v}}}{S}\lambda_{\text{f}}\right)$$

This thermal flux is then multiplied by the ratio of the contact area over the whole surface (i.e. F) to obtain the thermal flux over the whole billet surface.

The oxide scale is removed by a descaling process using high-pressure water sprays. The main heat exchange mechanism in this case is thermal convection:

$$\dot{q}_{\text{out}} = \alpha_{\text{w}}(T_{\text{w}} - T_{\text{s}})$$

4. Modelling the thin oxide scale

During the reheating process, the billets are exposed to oxide-scale formation. There are two main effects of oxide scale on heat transfer during transport: the effect of emissivity and the effect of scale thickness. The reason for the effect of emissivity is that the emissivity factor of the oxide scale differs from the emissivity factor of the billet material. For the emissivity factor of the primary oxide scale $\varepsilon_{\text{s}} = 0.6$ is used in the model, as suggested by [1]. The emissivity factor of the billet material is about $\varepsilon_{\text{b}} = 0.8$ and it varies depending on the material and on the temperature. The scale-thickness effect is a consequence of the different thermal properties of the oxide scale and the billet material. The main difference is in the thermal conductivity. It is suggested by [1] to take a 10 to 15 times smaller value for the thermal conductivity (λ_{s}) of the oxide scale than for the billet material (λ_{b}).

In order to use the finite-difference method, the billet is divided into a uniform rectangular mesh. To include the effect of oxide scale in the model, the mesh was refined. The oxide scale is much thinner (i.e. 1 mm) when compared to the size of the billet elements (i.e. 10 mm). If the mesh of all the billet elements was refined to the scale thickness, the number of calculation elements would increase and the calculation time would be prolonged. For this reason, the three-dimensional finite-difference equations were derived separately for the thin oxide scale as a shell around the billet (Fig. 2B). The side dimension of the oxide-scale elements, which are in contact with the

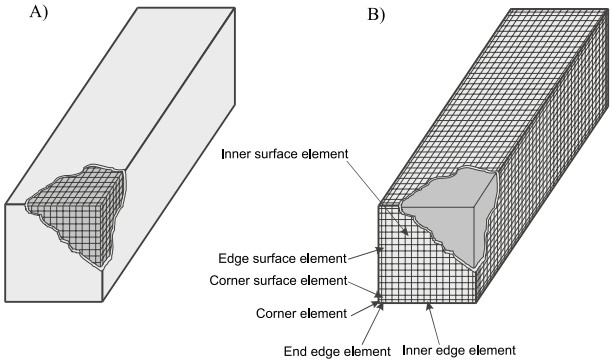

Fig. 2. (A) Billet with the oxide scale. (B) The oxide-scale mesh and basic elements.

billet elements, are the same as the corresponding billet surface elements (Fig. 2A), while the thickness of the oxide-scale elements are the same as the scale thickness. The developed equations for the scale allow the basic finite-difference model of the billet to remain unchanged. The connection between the elements of the billet surface and the oxide scale are represented by the thermal fluxes. This shell oxide-scale model also allows treating the air gap between the oxide scale and the billet material.

There are six basic oxide-scale elements for the rectangular geometry (Fig. 2B), for which equations have to be derived: the inner surface element, the edge surface element, the corner surface element, the inner edge element, the end edge element and the corner element. All the elements can be used for other surfaces, edges and corners with an appropriate change of parameters.

The oxide-scale surfaces were named A, B, C, D, E and F (Fig. 1). The elements on the surfaces were indexed two-dimensionally (i.e. surface A: (A,j,k), with index i constant, surface F: (F,i,j), with the index k constant). The intervals of the indexes were: $i \in [0, MX-1]$, $j \in [0, MY-1]$, $k \in [0, MZ-1]$.

Inner surface element: The inner surface element (j,k) of the oxide surface A is shown in Fig. 3A. The temperature $T_{A,j,k}$ in the next time interval $t+\Delta t$ can be calculated by the recursive equation from known values at time t:

$$T_{A,j,k}^{t+\Delta t} = a_s \Delta t \left[\frac{\dot{q}_{A\text{out}} + \dot{q}_{\text{billet},A,j,k}}{\lambda_s d} + \frac{T_{A,j-1,k}^t + T_{A,j+1,k}^t - 2T_{A,j,k}^t}{\Delta y^2} + \frac{T_{A,j,k-1}^t + T_{A,j,k+1}^t - 2T_{A,j,k}^t}{\Delta z^2} \right] + T_{A,j,k}^t$$

The thermal flux $\dot{q}_{\text{billet}}$ is calculated between the observed element of the oxide scale and the same positioned element of the billet surface. The thermal flux $\dot{q}_{A\text{out}}$ is a function of the element temperature and the boundary conditions. The derived element can be used in the other five surfaces (B, C, D, E, F) of the billet oxide scale after appropriate changes.

Edge surface element: The edge surface element $(0,k)$ of the oxide surface A is shown in Fig. 3B. The temperature $T_{A,0,k}$ in the next time interval $t+\Delta t$ can be calculated by the recursive equation from known values at time t:

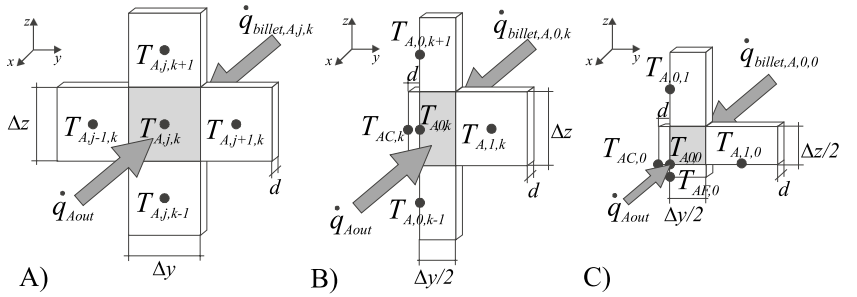

Fig. 3. (A) The inner surface element. (B) The edge surface element. (C) The corner surface element.

$$T_{A,0,k}^{t+\Delta t} = a_s \Delta t \left[\frac{\dot{q}_{A\text{out}} + \dot{q}_{\text{billet},A,0,k}}{\lambda_s d} + \frac{2(T_{AC,k}^t - T_{A,0,k}^t)}{d\,\Delta y} + \frac{2(T_{A,1,k}^t - T_{A,0,k}^t)}{\Delta y^2} + \frac{T_{A,0,k-1}^t + T_{A,0,k+1}^t - 2T_{A,0,k}^t}{\Delta z^2} \right] + T_{A,0,k}^t$$

Corner surface element: The corner surface element (0,0) of the oxide surface A is shown in Fig. 3C. The temperature $T_{A,0,0}$ in the next time interval $t + \Delta t$ can be calculated by the recursive equation from known values at time t:

$$T_{A,0,0}^{t+\Delta t} = a_s \Delta t \left[\frac{\dot{q}_{A\text{out}} + \dot{q}_{\text{billet},A,0,0}}{\lambda_s d} + \frac{2(T_{AC,0}^t - T_{A,0,0}^t)}{d\,\Delta y} + \frac{2(T_{A,1,0}^t - T_{A,0,0}^t)}{\Delta y^2} + \frac{2(T_{AF,0}^t - T_{A,0,0}^t)}{d\,\Delta z} + \frac{2(T_{A,0,1}^t - T_{A,0,0}^t)}{\Delta z^2} \right] + T_{A,0,0}^t$$

Inner edge element: The inner edge element (j) of the oxide edge of surfaces A and F is shown in Fig. 4A. The temperature $T_{AF,j}$ in the next time interval $t + \Delta t$ can be calculated by the recursive equation from known values at time t:

$$T_{AF,j}^{t+\Delta t} = a_s \Delta t \left[\frac{\dot{q}_{A\text{out}} + \dot{q}_{F\text{out}}}{\lambda_s d} + \frac{T_{F,MX-1,j}^t + T_{A,j,0}^t - 2T_{AF,j}^t}{d^2} + \frac{T_{AF,j-1}^t + T_{AF,j+1}^t - 2T_{AF,j}^t}{\Delta y^2} \right] + T_{AF,j}^t$$

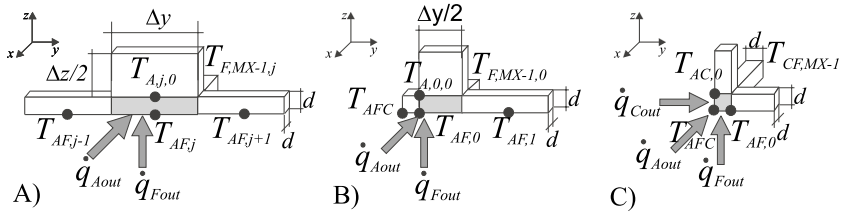

Fig. 4. (A) The inner edge element. (B) The end edge element. (C) The corner element.

End edge element: The end edge element (0) of the oxide edge of surfaces A and F is presented in Fig. 4B. The temperature $T_{AF,0}$ in the next time interval $t + \Delta t$ can be calculated by the recursive equation from known values at time t:

$$T_{AF,0}^{t+\Delta t} = a_s \Delta t \left[\frac{\dot{q}_{A\text{out}} + \dot{q}_{F\text{out}}}{\lambda_s d} + \frac{T_{F,MX-1,0}^t + T_{A,0,0}^t - 2T_{AF,0}^t}{d^2} + \frac{2(T_{ACF}^t - T_{AF,0}^t)}{\Delta y\, d} + \frac{2(T_{AF,1}^t - 2T_{AF,0}^t)}{\Delta y^2} \right] + T_{AF,0}^t$$

Corner element: The corner element of the surfaces A, C and F is shown in Fig. 4C. The temperature T_{ACF} in the next time interval $t + \Delta t$ can be calculated by the recursive equation from known values at time t:

$$T_{ACF}^{t+\Delta t} = a_s \Delta t \left[\frac{\dot{q}_{A\text{out}} + \dot{q}_{C\text{out}} + \dot{q}_{F\text{out}}}{\lambda_s d} + \frac{T_{AC,0}^t + T_{AF,0}^t + T_{CF,MX-1}^t - 3T_{ACF}^t}{d^2} \right] + T_{ACF}^t$$

4.1. Thermal flux between the billet and the oxide scale

The derived oxide-scale elements allow the main heat-conduction model of the billet to remain unchanged, regardless of whether the oxide scale is treated or not. The thermal exchange between both the scale element and the corresponding billet surface element is described by the thermal flux using the equation:

$$\dot{q}_{\text{billet},A,j,k} = \frac{\lambda_s}{d} (\vartheta_{MX-1,j,k} - \vartheta_{A,j,k}) \tag{1}$$

When the billet is discharged from the furnace, the oxide scale starts to cool faster than the billet material because of its different thermal properties. This causes the oxide scale to shrink faster. Therefore, it splits off from the billet and an air gap appears between the scale and the billet. This significantly changes the thermal flux and so it needs to be treated separately. The air-gap effect is shown in Fig. 5.

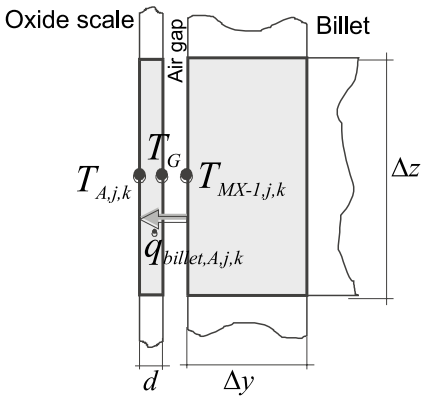

Fig. 5. The air gap between the oxide scale and the billet material.

The thermal flux $\dot{q}_{\text{billet},A,j,k}$ from the billet-surface element $(MX-1,j,k)$ to the oxide-scale element (A,j,k) can be divided into two fluxes: the $\dot{q}_1$ flux from $(MX-1,j,k)$ to T_G and the $\dot{q}_2$ flux from T_G to (A,j,k). The $\dot{q}_1$ can be calculated as radiation heat exchange between two infinite parallel planes [2], the radiation shape factor is unity since all the radiation leaving one plane reaches the other plane:

$$\dot{q}_1 = \frac{\sigma(T^4_{MX-1,j,k} - T^4_G)}{\frac{1}{\varepsilon_b} + \frac{1}{\varepsilon_s} - 1}$$

The $\dot{q}_2$ can be calculated as heat conduction inside the oxide-scale material:

$$\dot{q}_2 = \frac{\lambda_s}{d}(T_G - T_{MX-1,j,k})$$

The temperature $T_{A,j,k}$ of the oxide-surface element and $T_{MX-1,j,k}$ of the billet-surface element are known, the only unknown is the temperature T_G on the inner surface of the oxide scale. It can be calculated by solving the next equation on T_G:

$$\dot{q}_1 - \dot{q}_2 = 0$$

It can be solved numerically using a bisection method. As soon as we have the temperature T_G, as $\dot{q}_1 = \dot{q}_2 = \dot{q}_{\text{billet},A,j,k}$, the thermal flux $\dot{q}_{\text{billet},A,j,k}$ can be calculated.

5. Simulation results

The model was verified using real measurements with a thermal camera. The comparison between the measured and the calculated temperature field of the side surface of the billet is shown in Fig. 6. The comparison is made in two places, where the thermal camera measurements can be made. The measured temperature fields are not as rectangular as the billets are. The reason is in the slow thermal camera scanning speed while the billet is moving during the measurements. The billet in Fig. 6A is moving from right to left and the billet in Fig. 6B is moving from left to right, with respect to the recording position. Fig. 6A represents the temperature field in the 24th second of transport, and shows a non-uniform longitudinal temperature profile due to the distribution of water in the descaling system. Fig. 6B represents the measured and the calculated temperature field in the 50th second of transport.

Fig. 6. Comparison between measured and calculated thermal field of the billet.

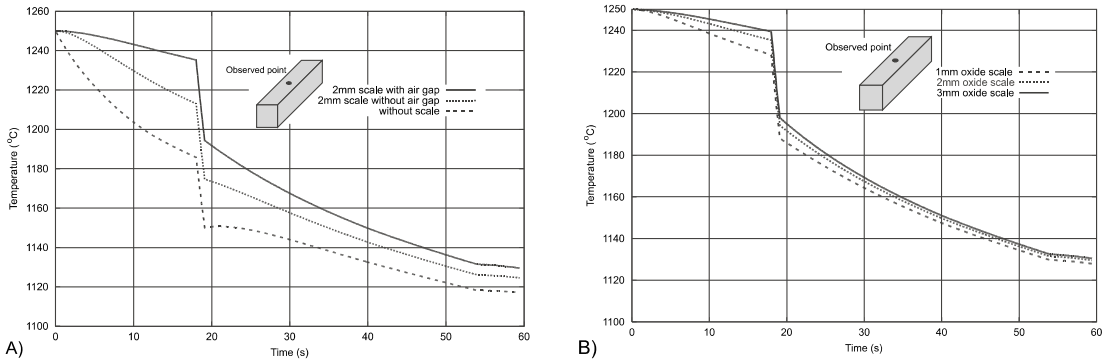

Fig. 7. Billet cooling: (A) simulation results considering the oxide-scale thickness and the air gap. (B) Simulation results for different scale thicknesses.

Fig. 7A shows the simulation results of a billet cooling during the transport using three different models. The first model simulates cooling without considering the oxide scale on the billet surface (curve 3). The second model assumes a 2 mm oxide scale (curve 2). The third model assumes both: the 2 mm oxide scale and the air gap between the scale and the billet (curve 1). The effect of the oxide scale is considered for the first 18 s of the transport path where the oxide scale is present. After the descaling, the cooling is simulated under equal conditions for all three curves and the differences can still be noticed in the billet temperature field at the end of the transport. It can be concluded that the oxide scale and the air gap between the oxide scale and the billet significantly affect the billet cooling during the transport and need to be considered in the model.

Fig. 7B shows the simulation results of billet cooling for three different scale thicknesses with the air gap present. Significant differences in temperature occur only in the first 18 s of billet transport, where the oxide scale is present. At the end of the simulations, the observed point temperatures become almost equal for all three scale thicknesses. It can be concluded that the effect of scale thickness would be noticed if the descaling process was at the end of the transport. In this particular case, where the scale is present just during the first 18 s of the transport, there is no effect of the scale thickness on the final temperature field of the billet.

6. Conclusion

The presented simulation model of billet transport from the reheating furnace to the rolling mill allows us to determine the three-dimensional temperature field in the billet. The model also considers the oxide scale on the billet. It was found that the oxide scale has a significant effect on the temperature field of the billet. The predictions of the model considering the oxide scale are in good agreement with the experimental data recorded with a thermal camera. The model will be used for the optimisation of a billet transport system. Further work is being carried out towards investigating the oxide-scale effect on the reheating process in the furnace, including the effect of the scale growth.

Acknowledgements

The authors thank the Inexa-Štore Steelworks and the Ministry of Science and Technology of Slovenia for the financial support of the project.

References

[1] W.C. Chen, I.V. Samarasekera, A. Kumar, E.B. Hawbolt, Mathematical modelling of heat flow and deformation during rough rolling, Ironmaking and Steelmaking 20 (2) (1993) 113–125.
[2] J.P. Holman, Heat Transfer, McGraw-Hill Book Company, New York, 1986.
[3] R. Siegel, J.R. Howell, Thermal Radiation Heat Transfer, McGraw-Hill Book Company, New York, 1981.
[4] M.N. Özisik, Heat Transfer, A Basic Approach, McGraw-Hill Book Company, Singapore, 1985.